

## Supporting Information for Analysis of Interactions in a Molecular Tunnel Junction

Shuai Chang<sup>1</sup>, Jin He<sup>2</sup>, Peiming Zhang<sup>2</sup>, Brett Gyarfas<sup>1</sup> and Stuart Lindsay<sup>1,2,3</sup>

<sup>1</sup>Department of Physics, <sup>2</sup>Biodesign Institute and <sup>3</sup>Department of Chemistry and  
Biochemistry, Arizona State University, Tempe, AZ 85287.

1. DC adjustment of the gap and mechanical interactions.
2. Preparation and characterization of monolayers of imidazole-2-carbamide on Au(111).
3. Preparation and functionalization of STM probes.
4. Large and small amplitude expressions for  $G_{AC}$ .
5. Calibration of the logarithmic amplifier.
6. Telegraph noise data for the conductance of single molecules.

### **1. DC adjustment of the gap and mechanical interactions.**

The time-response of the available computer-based current-distance curve collection function was too slow for collection of data at small gaps where the probe becomes unstable. For this reason, we replaced the commercial SPM controller with a field programmable gate array (FPGA) and programmed it to control the probe. The purpose of this custom system was to turn off servo control when a specified tunneling current had been reached and then proceed to withdraw the tip in a step wise fashion with a fixed step distance. In addition to the STM, the custom system incorporates a Field-Programmable Gate Array (PCIe-7842R, National Instruments), a computer running LabView (Version 8.5.1, National Instruments, Austin, TX) and PicoView (Version 1.8, Agilent, Chandler, AZ), and a signal breakout box from the STM controller. The system also exploits the  $\Delta Z$  BNC connector on the STM controller. This is an amplified input that allows an additional voltage to be added to the Z piezo high voltage. The system interface is programmed in LabView and will be referred to as the 'host VI'. The host VI is responsible for issuing API commands to PicoView. The Field-Programmable Gate Array (FPGA) is interfaced with the host VI through LabView.

The basic algorithm is as follows, a holding set-point is first set after approach. This is a current where there is no danger of the tip crashing on the surface. Next, the set-point is changed to an approach set-point. At this set-point the tip cannot be held stably without crashing after a time of approximately 500ms. Once the approach set-point is set the FPGA monitors the tunneling current from the breakout box at a sample frequency of 250 kHz. Once the tunneling current is greater than a predetermined current the FPGA signals the host VI to turn off the

servo. Once the FPGA receives confirmation that the servo is off a voltage from the FPGA is applied to the  $\Delta Z$  BNC which will move the tip in the Z direction by a user specified amount. The voltage will then be held for a user specified amount of time and then another step taken. The amount of withdrawal steps can be controlled by the user. After the specified number of withdrawal steps has been executed the FPGA signals the host VI to reset to the holding set-point and turn the servo back on. In addition to this automation the system concurrently records the tunneling current and the Z piezo voltage.

1a: Effects of attractive forces.

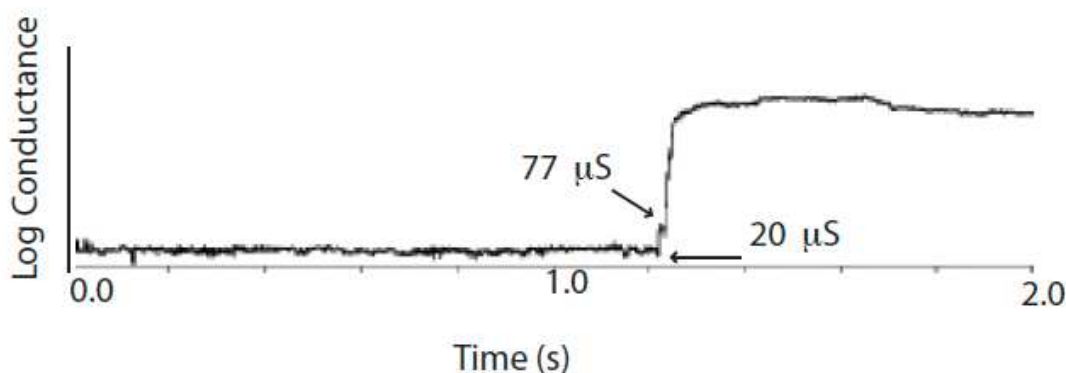


**Figure S1** shows how, even under servo control, a bare probe will jump into contact with a bare surface when the setpoint (here  $\sim 20 \mu\text{S}$ ) is near  $G_0$ . The gap conductance jumps to  $G_0$  and the climbs rapidly as the contact area increases.

1b. Effects of repulsive forces.

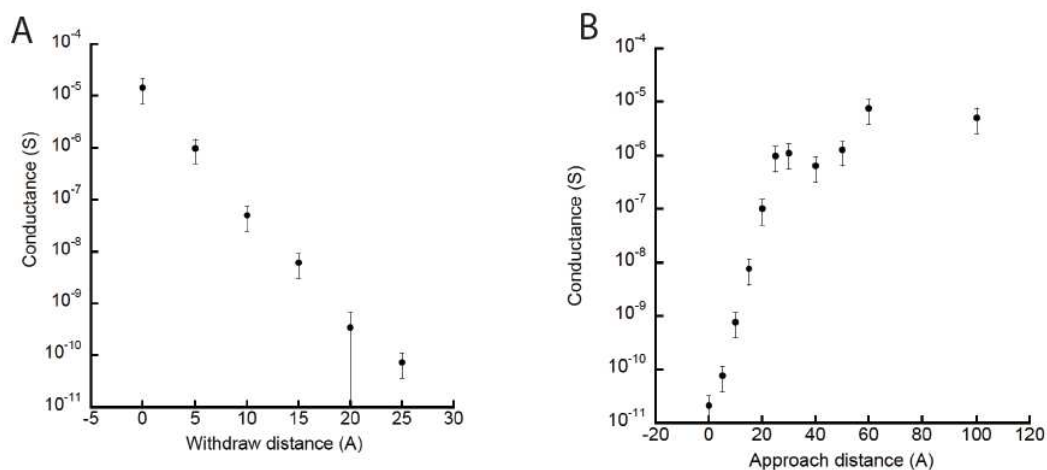


**Figure S2** showing conductance as a function of distance pulled back from  $7 \mu\text{S}$  (A) and as a function of distance moved forward from  $20 \text{ pS}$  (B). Data are for a bare gold probe and bare surface in  $1 \text{ mM PB}$  solution. The withdrawal data in A are

consistent with the 34 Å estimated from Fig. 2A to go from  $G_0$  to 6 pS. This gap is exaggerated by elastic interactions at high conductance. When the gap is closed (B) trapping of contamination often prevents the gap from closing, limiting the conductance to  $\sim 10^{-5}$  S. Data are extracted from at least 50 current-distance curves for each point.

## 2. Preparation and characterization of monolayers of 1*H*-imidazole-2-carboxamide on Au(111) substrates.

First, a stock solution (1 mM) of the imidazole-2-carboxamide was prepared by dissolving 4-(2-mercaptoethyl)-1*H*-imidazole-2-carboxamide (1.71mg, 0.01 mmole) into ethanol (10ml, HPLC grade). The gold substrates (Agilent Technologies) were annealed using a hydrogen flame. Immediately after that, the annealed substrate was immersed into the stock solution (2 mL) in a capped bottle for 24 hr, followed by thorough rinsing with ethanol and drying with nitrogen.

The monolayer was characterized by FTIR and Ellipsometry (Figure S3), XPS (Figure S4) and STM (Figure S5)

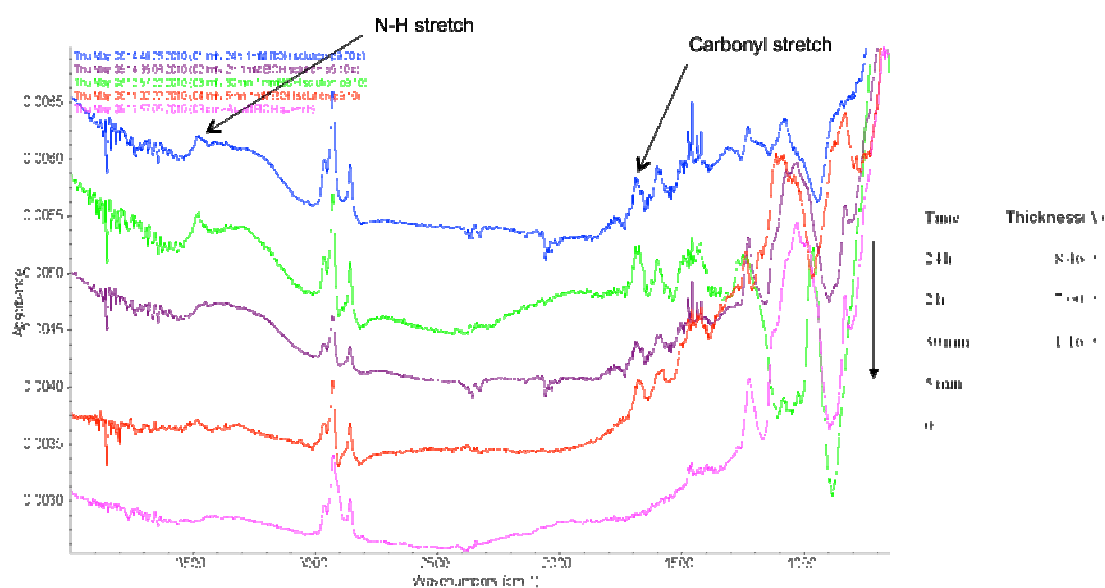
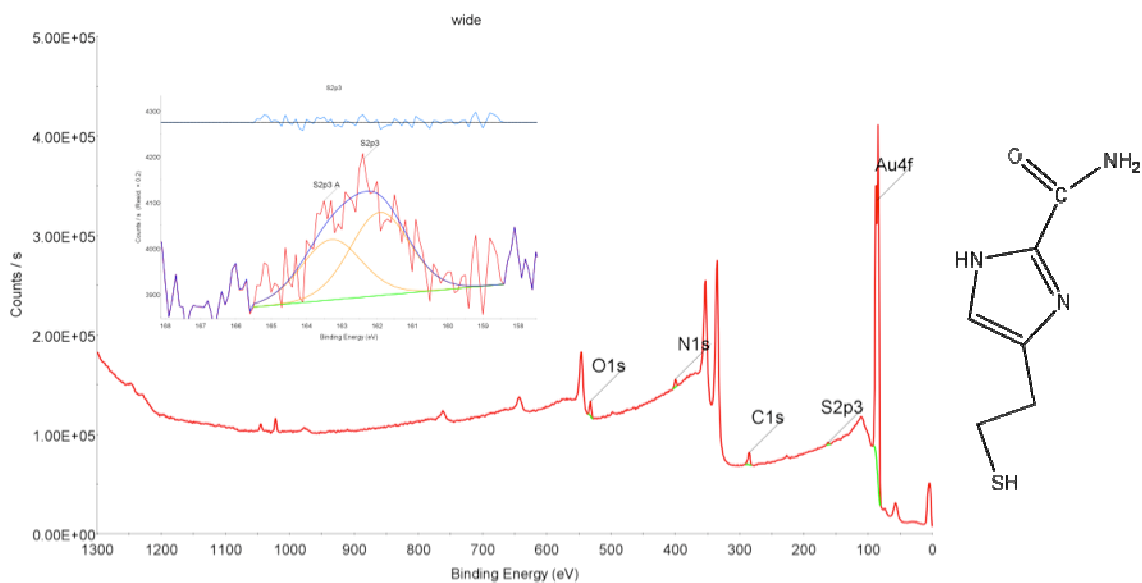


**Figure S 3.** FTIR spectra of the imidazole-2-carboxamide SAM as a function of exposure time (purple = 0, red = 5 min, violet = 30 min, green = 2h and blue = 24 h). The corresponding film thickness determined by ellipsometry is shown in the table at the right. The film saturates at a monolayer (8.5 Å).



Name	Start BE	Height Counts	Area (N)	At. %
Au4f	91.90	317037.56	106.16	53.99
S2p3	165.10	2152.39	6.85	3.49
C1s	291.10	11524.55	50.69	25.78
N1s	403.70	6688.05	14.34	7.29
O1s	535.90	12424.41	18.60	9.46

**Figure S 4.** XPS of the imidazole-2-carboxamide SAM. The S signal was very weak, and was fitted by the two states of sulfur. The 162 ev peak represents the BE of S2p3/2 bound to Au.

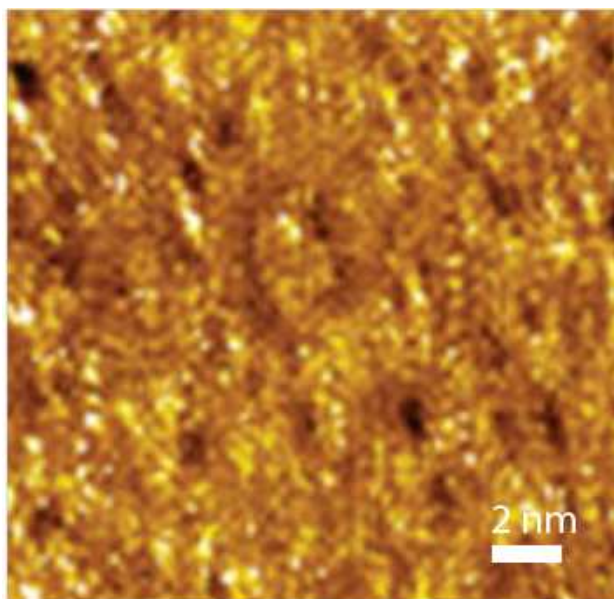


**Figure S 5.** High resolution STM image of the imidazole-2-carboxamide SAM showing a square adlayer of approximately 4 Å spacing. Image taken in PBS buffer, using a PtIr STM probe. Bias = 0.5V, setpoint current = 50 pA.

### 3. Preparation and functionalization of STM probes

Details of the etching and polyethylene coating of STM probes have been given before (see the supporting information for Huang et al.<sup>1</sup>). Briefly, 0.25 mm Au wire (99.999%) is etched in 1:1 conc. HCl: ethanol using a square wave of amplitude 27V and frequency 4.2 kHz. Freshly-prepared probes are coated with high-density polyethylene as described previously<sup>2</sup>, rinsed in ethanol for 10 min and then submerged in the stock solution of 4-(2-mercaptoethyl)-1*H*-imidazole-2-carboxamide (1.71mg, 0.01 mmole) into ethanol (10ml, HPLC grade) for 8 h. The etch profile of the probes is critical in obtaining a high yield of functionalized probes without interference from the polyethylene coating. A rounded end with a very sharp asperity yields almost 100% of functionalized probes, as verified by tunneling measurements on a bare gold substrate where tunneling signals characteristic of one molecule in the gap signal the successful functionalization.

### 4. Large and small amplitude expressions for $G_{AC}$ .

#### 4.1 AC modulation

We apply a sine wave of 1.5 mV amplitude and 2kHz frequency to the Z PZT using a summing port on the microscope controller (Gain = 21.5). The PZT sensitivity was calibrated using STM images of single atom steps on Au(111) yielding 1.6 nm/V. Thus the modulation is  $1.5 \times 10^{-3} \times 21.5 \times 16 = 0.516$  Å. 21.5 is the amplifier, the input AC amplitude will be amplified 21.5 times in the real controller system.

## 4.2 Calculation of $G_{AC}$ :

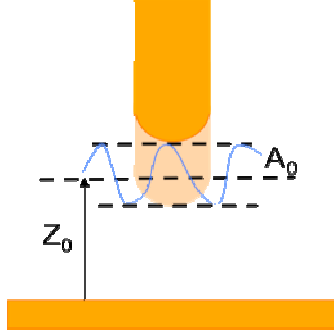


**Figure S6.** Showing the STM measurement applied AC modulation.  $Z_0$  is the distance between two electrode,  $A_0$  is the AC amplitude.

First we have:

$$\begin{aligned}
 Z &= Z_0 + A_0 \sin(\omega t), \\
 G &= G_0 \exp(-\beta(Z_0 + A_0 \sin(\omega t))) \\
 &= G_0 \exp(-\beta Z_0) (1 - \beta A_0 \sin(\omega t) + \frac{1}{2} (\beta A_0 \sin(\omega t))^2 \\
 &\quad - \frac{1}{6} (\beta A_0 \sin(\omega t))^3 + \frac{1}{24} (\beta A_0 \sin(\omega t))^4 - \Delta)
 \end{aligned}$$

Using the standard expansions for  $\sin^2$ ,  $\sin^3$  and  $\sin^4$ , we

$$\begin{aligned}
 G &= G_0 \exp(-\beta Z_0) \left[ \left( 1 + \frac{\beta^2 A_0^2}{4} + \frac{\beta^4 A_0^4}{64} \right) - (\beta A_0 + \frac{\beta^3 A_0^3}{8}) \sin \omega t \right. \\
 \text{have} \quad &\left. - \left( \frac{\beta^2 A_0^2}{4} + \frac{\beta^4 A_0^4}{48} \right) \cos 2\omega t + \frac{\beta^3 A_0^3}{24} \sin 3\omega t + \frac{\beta^4 A_0^4}{192} \cos 4\omega t - \Delta \right]
 \end{aligned}$$

$$G_{DC} = G_0 \exp(-\beta Z_0) \left( 1 + \frac{\beta^2 A_0^2}{4} + \frac{\beta^4 A_0^4}{64} \right)$$

$$G_{AC} = G_0 \exp(-\beta Z_0) \left( \beta A_0 + \frac{\beta^3 A_0^3}{8} \right) \sin \omega t$$

For  $A_0 = 0.516 \text{ \AA}$  and  $\beta = 0.8 \text{ \AA}^{-1}$  the higher terms are quite small, ( $\frac{\beta^2 A_0^2}{4}$  is 0.04,

$\frac{\beta^3 A_0^3}{8}$  is 0.008...), so we can omit them. We get:

$$G_{DC} = G_0 \exp(-\beta Z_0)$$

$$G_{AC} = G_0 \exp(-\beta Z_0) \beta A_0$$

Thus:

$$G_{AC} = G_{DC} \beta A_0$$

### 5. Calibration of the logarithmic amplifier.

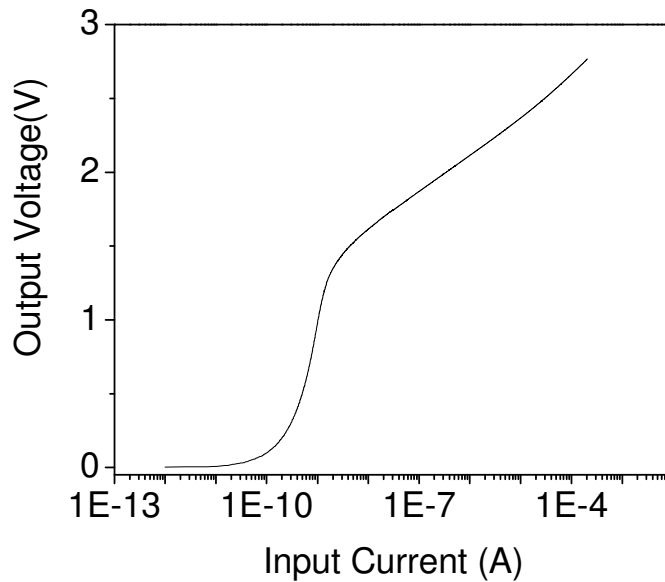


**Figure S 7.** The log amplifier was calibrated by loading the probe with resistors of 2G $\Omega$ , 1 G $\Omega$ , 500M $\Omega$ , 100 M $\Omega$ , 50 M $\Omega$ , 10 M $\Omega$ , 5 M $\Omega$ , 1 M $\Omega$ , 500 k $\Omega$ , 100 k $\Omega$ , 50k $\Omega$  and 15 k $\Omega$  to produce the calibration curve shown above. Calibration was checked frequently because the log amplifier is not temperature compensated.

## 6. Telegraph noise data for the conductance of single molecules.

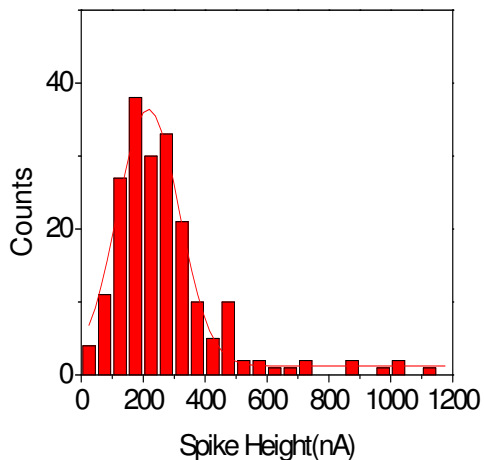


**Figure S 8.** Distribution of telegraph noise spike heights above the background setpoint current of 338 nA (conductance = 675 nS) for a bare probe and a surface functionalized with imideazole-2-carboxamide (in 1 mM PB).

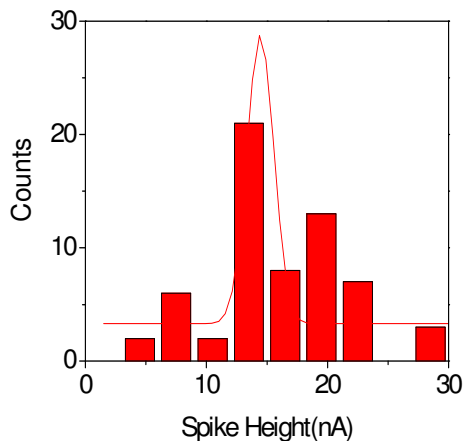


**Figure S 9.** Distribution of telegraph noise spike heights above the background setpoint current of 3.2 nA (conductance = 6.4 nS) for a probe and a surface both functionalized with imideazole-2-carboxamide (in 1 mM PB).

## References

- 1 Huang, S., He, J., Chang, S., Zhang, P., Liang, F., Li, S., Tuchband, M., Fuhrman, A., Ros, R., & Lindsay, S.M., Identifying single bases in a DNA oligomer with electron tunneling. *Nature Nanotechnology* 5, 868-873 (2010).



- 2 Visoly-Fisher, I., Daie, K., Terazono, Y., Herrero, C., Fungo, F., Otero, L., Durantini, E., Silber, J.J., Sereno, L., Gust, D., Moore, T.A., Moore, A.L., & Lindsay, S.M., Conductance of a biomolecular wire. *Proc. Nat. Acad. Sci.* 103, 8686–8690 (2006).